Aerosol size distribution from inversion of solar radiances and measured at ground-level during SPALI10 campaign

Jesús Fernández-Gálvez[1,2], Juan Luis Guerrero-Rascado[1,2,3], Francisco Molero[4], Hassan Lyamani[1,2], María Aranzazu Revuelta[4], Francisco Navas-Guzmán[1,2], Mariano Sastre[4], Juan Antonio Bravo-Aranda[1,2], Alfonso Javier Fernández[4], María José Granados-Muñoz[1,2], Francisco Javier Gómez-Moreno[4], Francisco José Olmo[1,2], Manuel Pujadas[4], Lucas Alados-Arboledas[1,2]

Abstract — A comparison of columnar versus ground-level measurements of aerosol size distribution is presented. Measurements were taken during the SPALI10 (SPAin Lidar Intercomparison 2010) field campaign at Madrid (40.45ºN, 3.73ºW, 663 m asl) from 18 October to 5 November 2010 within the frame of the EARLINET-ASOS project. Monitoring period included aerosol measurements of size distribution as well as chemical composition. Both combined Scanning Mobility Particle Sizer (TSI SMPS 3936) and an Optical Particle Counter (GRIMM 1108) were used for determining aerosol size distribution ranging from 15 nm to 10 μm. Additionally, the column integrated characterization of the atmospheric aerosol was provided by a sun tracking photometer (Cimel CE-318-4) using a methodology based on non-spherical particles. The instrument provides solar extinction measurements at 340, 380, 440, 670, 870 and 1020 nm, and sky radiance measurements at 440, 670, 870 and 1020 nm using the almucantar and principal plane configurations. The sky radiance measurements in conjunction with solar direct irradiance measurements at several wavelengths were used to retrieve the aerosol size distribution. Measurements at ground-level were compared with the columnar estimates using the retrieved scale height values provided by lidar profiles. Relevant features arising from results showed the complex role of aerosol in urban atmospheres.

Keywords — Atmospheric aerosol size distribution, lidar, lidar derived scale height, solar radiation

1 INTRODUCTION

Atmospheric aerosols have a significant impact on the Earth's surface radiative balance due to the direct effect from scattering and absorption of direct solar radiation, and indirectly by acting as condensation nuclei influencing cloud microphysics. Nevertheless, uncertainties in concentration, size, composition and vertical distribution throughout the atmosphere make difficult to quantify their effect on the overall energy budget. The currently increasing interest on atmospheric aerosols is twofold, their impact on climate and health. Therefore there is an interest on monitoring and characterizing the atmospheric aerosol properties. As for many other atmospheric variables, aerosols can widely vary in space and time, adding an additional challenge to their characterization.

1. *Centro Andaluz de Medio Ambiente (CEAMA), Universidad de Granada, Av. del Mediterráneo, 18006 Granada, Spain*
First author e-mail: jesusfg@ugr.es
2. *Departamento de Fisica Aplicada, Universidad de Granada, Campus de Fuentenueva, 18071 Granada, Spain*
3. *Centro de Geofisica de Évora (CGE), Universidade de Évora, Rua Romão Ramalho 59, 7000 Évora, Portugal*
4. *Centro de Investigaciones Energéticas, Medioambientales y Tecnológicas (CIEMAT), Av. Complutense 22, 28040 Madrid, Spain*

One of the simplest and most accurate monitoring systems is passive ground-based remote sensing instruments based on solar radiation measurements (sun-photometers). They are currently deployed over the land surface as a network (AERONET, Aerosol Robotic Network, http://aeronet.gsfc.nasa.gov) [1], providing measurements of aerosol properties for the entire atmospheric column. This approach uses an inversion algorithm to retrieve the columnar optical and microphysical properties of aerosols such as aerosol optical depth (AOD), single scattering albedo, asymmetry factor and volume size distribution. Nevertheless it is important to note that most inversion algorithms assume a vertically homogeneous atmosphere with constant aerosol characteristics along the entire column. Since the atmosphere normally differs from that, an unknown error in the retrieved variables is introduced. Estimates of AOD can also be obtained from surface measurements scaled to height using aerosol backscatter profiles from lidar measurements, but aerosol extinction next to the surface happens to be essential in this later case [2]. The connection between the columnar aerosol size distribution and some features of the atmospheric vertical profile is clear but unfortunately the methods to obtain the microphysical parameters of a disperse system of particles based on know extinction data is an ill-

posed inverse problem [3]. Moreover, the inversion technique produces a particle size distribution restricted in range because AOD is measured in a limited radius interval. Therefore, it is important to account for the assumptions and numerical limitations of the inversion procedures when estimating particle physical properties [4], [5].

Bokoye et al. [6] studied the effect of vertical averaging comparing data from a Passive-Cavity-Aerosol-Scattering-Probe and sun-photometer retrieved size distributions using scale heights measured by a lidar system. Their results were only partially satisfactory due to some readjusting of scale heights. Molero et al. [7] compared aerosol volume size distribution measured by sun-photometry and in-situ instrumentation, concluding that, when convective turbulence dominates and in absence of long-range transport, the column and surface size distributions can be related by means of the scale height provided by a lidar system. Conversely, the lack of homogeneity in the aerosol vertical distribution deviated columnar from surface properties.

This work presents a comparison of columnar aerosol volume size distribution from inversion of solar radiances and in-situ measurements for different atmospheric scenarios occurring during the SPALI10 campaign at Madrid (Spain). Measurements of aerosol size distribution ranging from 15 nm and 10 μm were taken using a Scanning Mobility Particle Sizer and an Optical Particle Counter. Retrieved scale heights were provided by simultaneous measurements of backscatter lidar profiles. Independent data from column integrated characterization of the atmospheric aerosol provided by a sun tracking photometer were used for comparison. The purpose of this study is to combine the information retrieved from in-situ measurements in the surface boundary layer and the information retrieved above the vertical column. That can be interpreted as integrated in the case of a cimel radiometer or vertically resolved as in the case of a lidar system. For this purpose a data set including information from the different sources has been selected. Three representative scenarios fulfilling the requirements were analyzed.

This paper is organized as follows. Section 2 is devoted to a brief description of the experimental site and the instrumentation and methodologies used in this study. Section 3 is focused on results and discussion. Here a brief characterization of the prevailing synoptic situation during selected days is presented together with an analysis regarding in-situ, columnar and vertically-resolved measurements. Finally, section 4 presents the main conclusions.

2 Instrumentation and Methodology

2.1 Experimental Site

Experimental data were taken during the SPALI10 (SPAin Lidar Intercomparison 2010) field campaign at Madrid (40.45°N, 3.73°W, 663 m asl) from 18 October to 5 November 2010 within the framework of the EARLINET-ASOS project (European Aerosol Research LIdar Network - Advanced Sustainable Observation System, www.earlinet.org. The aim of the campaign was to compare simultaneous lidar measurements from several network stations with a reference lidar system from CNR-IMAA (Potenza, Italy). At the same time, an extensive dataset from both ground-level in-situ measurements and remote sensing techniques was collected for characterizing aerosol optical and microphysical properties.

The Madrid metropolitan area is located in the center of the Iberian Peninsula, bordered to the north–northwest by a high mountain range (Sierra de Guadarrama) 40 km from the city, and to the northeast and east by lower mountainous terrain. The population of the metropolitan area of Madrid is nearly 6 million inhabitants, with a car fleet of almost 3 million vehicles. Since its industrial activity consists essentially of light factories, the Madrid atmosphere is typically urban, fed by traffic emission and also by domestic heating in winter. Previous studies of air pollution episodes in the Madrid air basin have characterized their driving meteorological conditions and their typical transport patterns [8], [9], [10]. The general synoptic situation leading to the occurrence of episodic events corresponds in winter to stagnant anticyclone conditions, light winds and clear-sky conditions, with the usual formation of radiative nocturnal surface inversions. In spite of the local-regional transport pattern, the distance between the Madrid metropolitan area and other significant urban or industrial areas in Spain (around 200 km) allows for the study of its atmosphere as a typical urban plume. Long-range transport episodes significantly affecting aerosol concentrations in the Madrid region are usually limited to Saharan mineral dust intrusions [11]. The arrival of Atlantic or polar air masses generally has a cleansing effect on the atmosphere, significantly reducing particulate matter levels.

The experimental site at CIEMAT (Centro de Investigaciones Energéticas, Medioambientales y Tecnológicas) is located in the Madrid North West city outskirts and it can be considered as an urban background or suburban site. It is situated downwind of the city for North to South West wind directions and downwind of a great forested area for West to North West wind directions. Simultaneous vertical profiles and surface aerosol concentration measurements were carried out at the site with the instruments described below.

2.2 In-Situ Instrumentation

At ground level, the temporal evolution of particle number, sulfate and mass concentration for particles smaller than 10, 2.5 and 1 μm diameter (PM_{10}, $PM_{2.5}$ and PM_1) were monitored at the experimental site. Time series of particulate sulfate on PM_1 were obtained by means of a Thermo 5020 sulfate particulate analyzer [12] at 20 min time resolution. The instrument reduces sulfate aerosol by thermal catalysis and analyzes the resulting sulfur dioxide gas by pulsed fluorescence. Laboratory conversion efficiencies have been proved to be higher for ammonium sulfate than for mineral-type sulfates. The measurements were corrected by comparison against daily filter-based measurements.

Particulate nitrate concentrations on $PM_{2.5}$ were measured by a Rupprecht and Patashnick Series 8400N Ambient Particulate Nitrate Monitor every 10 min [13]. This instrument comprises a pulse generator for the collection and vaporization of the particulate matter and a NOx pulse analyzer, mainly measuring mineral-type nitrates associated with the ammonium. These measurements were also corrected by comparison with daily filter-based measurements.

Aerosol size distribution was continuously monitored at ground level. Dry ambient sub-micrometer size distributions were monitored at the site by using a Scanning Mobility Particle Sizer (TSI SMPS 3936), combining a long Differential Mobility Analyzer (DMA) and a Condensation Particle Counter (CPC model 3775) working in the scanning mode [14]. This particle spectrometer uses the relation between the particle mobility and the diameter to calculate the particle size [15]. Before entering the DMA the sample is dried by a nafion drier, and particles are neutralized by a Kr-85 radioactive source. Once in the DMA, particles are classified according to their electrical mobility and then counted by the CPC. Data were obtained in the size range of 14.5–604 nm by using rates of 0.3 and 3.0 1 min^{-1} for aerosol and sheath flows, respectively. Volume size distribution for sub-micrometer aerosols was calculated by assuming spherical particles. Datasets were also corrected for losses caused by diffusion processes inside the instrument [16].

On a larger particle size range, an Optical Particle Counter (GRIMM 1108) was used, providing particulate counts distributed in 15 channels (0.15, 0.2, 0.25, 0.325, 0.4, 0.5, 0.8, 1.0, 1.5, 2.0, 2.5, 3.75, 5, 7.5 and 10 μm) by 90° laser light scattering. The ambient air, drawn into the unit, passes through a flat laser beam, produced by a laser diode and the scattered signals are detected by a multichannel pulse height analyzer for size classification. These data, in the form of particle counts, were converted to a volume distribution based on the particulate matter radius or a mass distribution using hardware coded particulate density [17].

The GRIMM and the SMPS overlap in the size range from 0. 15 μm (lower size end of the GRIMM) to 0.661 μm (upper size end of the DMA) resulting in a 22 bin overlap region spanning with Stokes radius (D_p) in the range $0.15 < D_p < 0.661$ μm for DMA and a 6 bin overlap region spanning $0.15 < D_p < 0.5$ μm for the GRIMM. Therefore, it is possible to obtain a single plot for number distributions between 0.015 to 10 μm by joining the data from both instruments assuming that the radius of a particle can be determined by measuring different physical properties such as light scattering or electrical mobility. The SMPS classifies particles according to their electrical mobility, considering that particles of equal D_p and carrying the same electrical charge will have the same electrical mobility. Hence, for spherical particles, the electrical mobility radius would equal D_p. Size distributions based on light scattering also use D_p which is independent of density. For spherical particles, the radius given by optical particle counters will equal D_p if light absorption is negligible and the refractive index is constant for the GRIMM distribution. Volume distributions ($dV/d\log(D_p)$) were calculated assuming that aerosol particles were spheres with a radius equal to the centre radius of each bin measured by the instruments.

2.3 Aerosol Columnar Instrumentation (Cimel)

The column integrated characterization of the atmospheric aerosol was performed by means of an automatic sun tracking photometer Cimel CE-318-4. The Cimel radiometers are described in detail in [1]; however, a brief description is given here. This instrument makes direct sun irradiance measurements with a 1.2° full field of view every 15 min at 340, 380, 440, 670, 870, 940 and 1020 nm. It takes about 8 s to scan all seven wavelengths, with a motor-driven filter wheel positioning each filter in front of the detector. These solar extinction measurements are then used to compute AOD at each wavelength except for the 940 nm channel, which is used to retrieve total column water vapour. Calibration of the instrument is regularly performed at Sierra Nevada (2200 m asl), at least twice a year, using the Langley plot technique. On the other hand, an integrating sphere is used to calibrate the instruments for radiance measurements [18].

The AOD is derived from the total optical depth obtained from direct sun-photometer measurements data using the appropriate calibration constant and subtracting the Rayleigh optical depth as well as the O_3 and NO_2 absorption optical depths [19]. Rayleigh, NO_2 and O_3 optical depths as well as optical air masses corresponding to the different constituents were computed from the equations given by Gueymard et al. [20]. For ozone column contents, values measured at El Arenosillo (37.1°N, 6.7°W, 17 m asl) with a Brewer MK-III were used. The NO_2 column contents were obtained from the midlatitude

model atmospheres in LOWTRAN7code [21]. The combined effects of uncertainties in calibration, atmospheric pressure, and total ozone amount result in a total uncertainty of about 0.010 in computed AOD (which is spectrally dependent with the higher errors in the UV [22]). Estellés et al. [23] compared AOD values derived from six cimel radiometers operating simultaneously together in a field experiment and found that the aerosol optical values from 380 to 1020 nm agreed to within 0.015 RMS, which is similar to the estimated level of uncertainty in AOD retrievals.

For the retrieval of aerosol optical properties, cloud-contaminated measurements were removed by using the cloud screening method by Smirnov et al. [24], which uses the difference of AOD between two consecutive measurements as a criterion determining the clear-sky condition. Even if data pass the threshold screening test, only data within three standard deviations from the mean were considered in order to further reduce uncertainties induced by cloud contamination. This technique relies on the greater temporal variance of cloud optical depth versus AOD, therefore temporally and spatially uniform cloud may at times be misidentified as cloud-free.

The sky radiance measurements, performed at the almucantar and principal planes at 440, 675, 870, and 1020 nm together with solar direct irradiance measurements at the same wavelengths, were used to retrieve the aerosol single-scattering albedo, phase function, aerosol optical thickness and the volume size distribution (dV(r)/dlnr (cm^3cm^{-2})) using the SKYRAD.pack software. This software package consists of a radiative transfer code as well as linear and nonlinear inversion components [25] based on spherical particle assumption. However, for the accurate retrieval of aerosol properties from sky radiation measurements, the influence of nonsphericity was also included for improving retrievals for large dust particles [26], [27].

2.4 Atmospheric Aerosol Profiling (Lidar)

Lidar measurements where taken with a Raman lidar model LR331D400 (Raymetrics S.A., Greece). The Raman Lidar system is configured in a monostatic biaxial alignment pointing vertically to the zenith. The transmitter of the lidar system is a pulsed Nd:YAG laser with fundamental emission at 1064 nm, and additional emissions at 532 and 355nm by using second and third harmonic generators. Output energies are 110, 65 and 60 mJ at 1064, 532 and 355 nm respectively, and pulses of 7 to 9 ns can be fired with a pulse repetition frequency of 1, 2, 5 and 10 Hz. The receiving system consists of a 0.4-meter diameter Cassegrain telescope and a wavelength separation unit with dichroic mirrors, interferential filters and a polarization cube, that discriminates seven channels corresponding to elastic wavelengths (1064, 532 parallel-polarized, 532 perpendicular-polarized and 355 nm), and to nitrogen and water vapour Raman-shifted wavelengths (387, 408 and 607 nm). Raman signals were not used in this study. The optics set-up is such that the maximum overlap is reached at about 400 m above the instrument.

The elastic lidar signal provides the aerosol backscatter coefficient using inversion methods. The basis of the technique is the elastic lidar equation which describes the return signal taking into account both atmospheric and instrumental parameters. From this signal aerosol backscatter profiles have been retrieved using the Klett-Fernald-Sasano's algorithm [28], [29], [30], [31], [32], [33]. A detailed description of retrieval method applied to backscatter lidar data can be seen in [34]. The retrieval of backscatter coefficient profiles, using Klett's algorithm, requires the use of a modelled value for the lidar ratio (i.e., the ratio between aerosol extinction and backscatter coefficient). Lidar backscattered signal was registered in 1-min integrated time and with a vertical resolution of 7.5 m.

2.5 Data Retrieval Procedures (Scale Heights)

In order to compare the column-integrated volume size distributions provided by the sun-photometer with the one obtained from the near-surface, several conversions are required. The two techniques measure different quantities; remote sensing is sensitive to the aerosol optical properties of the entire column, while in-situ instruments measure the aerosols at ground-level in one location, which may not be representative of the distributed aerosol in the total boundary layer. The distributions obtained by in-situ instrumentation at surface level (in $\mu m^3\ cm^{-3}$) are converted into columnar distribution ($\mu m^3\ cm^{-2}$) for comparison with sun-photometer retrievals by means of the so-called scale height, H. The computed H corresponds to the altitude where the integrated extinction is equal to $1\text{-}e^{-1}$ of the retrieved AOD for a given lidar profile. It arises from the simplified distribution of aerosol particles in the atmosphere used by most radiative transfer models, where it is assumed an exponential attenuation of atmospheric aerosol concentration with height. The distribution of aerosol particles with height is described by means of exponential profiles given by

$$N(h) = N(0)e^{-\left(\frac{h}{H}\right)} \qquad (1)$$

where h is the altitude above ground and H is the scale height, which describes the slope of the profile. Therefore, the integration of the whole profile distribution results in the surface concentration ($N(0)$) multiplied by H. Nevertheless this exponential approximation is not always valid, especially when the vertical homogeneity of the atmosphere is reduced. For example, Guerrero-Rascado et al. [35] reported an extreme Saharan dust

outbreak with a complex aerosol layering very different from an exponential decay (up to 83% of AOD located on a layer between 2.5 and 5.5 km asl). Their computations revealed that the lack of knowledge of real aerosol vertical distribution implies an overestimation of heating rate in the lower troposphere, especially within the PBL, and a marked underestimation in the free troposphere where long-range transport of aerosol particles takes place. Therefore, the knowledge of vertical distribution plays an important role in computations of the atmospheric heating rates.

Because our analyses are limited to daytime, and therefore the Raman method [36] to derive an independent extinction profile is not applicable, an alternative definition based on backscatter profiles is preferred:

$$\int_0^H \beta_{aerosol(z)dz=\left(1-e^{-1}\right)} \int_0^\infty \beta_{aerosol}(z)dz \qquad (2)$$

where $\beta_{aerosol}$ is the aerosol backscatter coefficient, H is the scale height and z is the altitude. The aerosol backscatter profile is computed by means of the aforementioned Klett-Fernald-Sasano´s method using a height-independent lidar ratio value as input (50 sr). The proposed method to derive the H assumes the absence of stratospheric aerosols and a planetary boundary layer homogeneously mixed between the ground and the height at which the lidar overlap factor is close to 1.

2.6 Meteorological Data

Meteorological information from a permanent tower installed at the site was continuously monitored. It included wind direction and speed at 52 m agl, precipitation and solar radiation at 31 m agl, temperature and humidity at 4 m agl and pressure at ground level. Additionally, radio sounding data twice a day (close to midnight and midday) were also available.

2.7 Backward trajectories

Backward trajectories have been calculated to determine the origin and the pathway of the air masses that affect the site. The HYSPLIT.4 (Hybrid Single Particle Lagrangian Integrated Trajectory) model developed by the NOAA's Air Resources Laboratory (ARL) [37], [38], [39] is used to calculate five-day backward trajectories of air masses coming to Madrid at six different altitudes above ground-level (500, 1000, 2000, 3000, 4000 and 5000 m agl) using the vertical wind component. This model uses the Global Data Analysis System, (ftp://www.arl.noaa.gov/pub/archives/gdas1/) meteorological files as data input with a spatial resolution of 1°×1° every 3 h generated and maintained by ARL.

3 Results and Discussion

3.1 Synoptic Situation

The meteorological analysis of the studied period shows a synoptic situation mainly governed by high-pressure systems over the Iberian Peninsula except for the last three days of October. During 27–28 October 2010 the high-pressure system extended from the peninsula toward North Africa. This situation blocks the entry of air masses from the Atlantic and promotes stagnation, reducing the ventilation of the atmosphere at the experimental site. The pressure gradient at the surface was very low and consequently there was an absence of wind with clear and dry day conditions. The analysis of the backtrajectories provided by the HYSPLIT model (not shown) indicates low circulation and recirculation at lower levels with some Atlantic influence at higher altitudes. Temperature near the surface varied from 10 to 20 °C and relative humidity from 10 to 60%. After these days there was a three days rain episode ending on 31 October, it produced a wash out of the atmosphere over Madrid after the previous stagnation period. In the beginning of November, the Azores high-pressure system dominated over the peninsula. Particularly from 2 to 4 November 2010, these high pressures permitted the entry of air masses from the Atlantic. Pressure gradients and winds were higher on the 2 with and slightly increase in surface pressure until November the 4. Temperatures at the surface ranged from 10 to 22 °C and relative humidity from 45 to nearly 100%. The backtrajectories from HYSPLIT crossed over the Atlantic without so much mixing between levels. Thermal inversion also occurred in the morning during these days but a higher altitude, 1330 and 850 m agl at 11:00 UTC for the 2 and 4 respectively.

3.2 In-Situ Particle Concentration

Although the measurement campaign expanded from 18 October to 5 November 2010, only data from 26 October are used here in order to focus results from the two synoptic scenarios in between the rain period indicated above. The temporal evolution of nitrate and sulphate concentration as well as PM_{10}, $PM_{2.5}$ and PM_1 mass concentration at the surface are shown in Figs. 1 and 2. The local pollution events produced by traffic rush hours, normally between 7:00 and 9:00 local time, but sometimes extending until midday, are clearly identified by sharp peaks of nitrate and PM_{10}. Sulphate as well as $PM_{2.5}$ and PM_1 show a similar trend, but less pronounced. Between these pollution peaks, the background pollution levels increased from day-to-day between 26 and 29 October due to stagnation of the air mass. Nitrate particle concentration during 27–28 October reached values above 8 μg m^{-3} during the traffic rush hours, and sulphate slightly increased from less than 1 up to nearly 1.5 μg m^{-3} during this period. As a result,

there was an increase of aerosol concentration near the surface, reinforced by the presence of a low level thermal inversion at around 300 m agl during the morning hours. Particularly for PM_{10}, the daily average concentration was above the limit established by the European Union (> 50 μg m^{-3}). On the other hand, the synoptic situation between 31 October and 5 November allowed the cleaning of the atmosphere from day-to-day, with lower than 4 μg m^{-3} nitrate particle concentration during rush hours, and also smaller PM_{10}, $PM_{2.5}$ and PM_1 mass concentration, specially for PM_{10}, with nearly half values compared to those before the rain episode. The results are consequence of the changes in synoptic situation, where the presence of a stagnation increase particle concentration levels and the inflow of Atlantic air masses avoid the accumulation of pollution from previous days, thus reducing particle concentration near the surface.

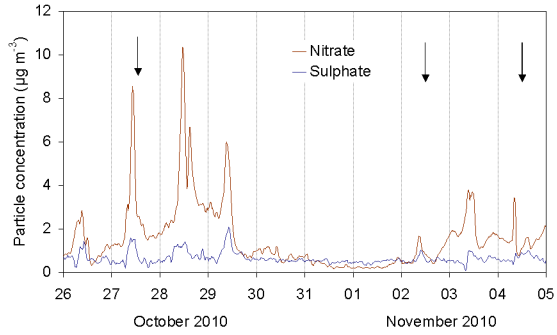

Fig. 1. Nitrate and sulphate concentration at the surface from 26 October to 5 November 2010. Arrows indicate selected dates analysed further in detail.

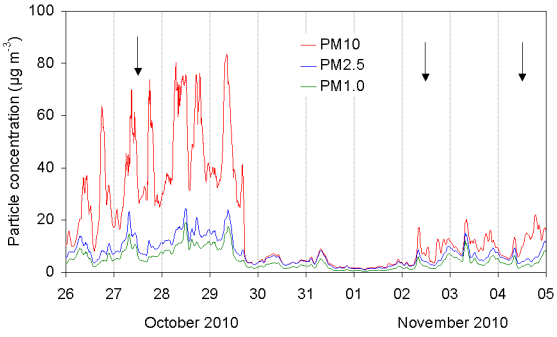

Fig. 2. Mass concentration for particles smaller than 10, 2.5 and 1 μm diameter from 26 October to 5 November 2010. Arrows indicate selected dates analysed further in detail.

Fig. 3 shows the aerosol volume size distribution vs. radius between 0.01 and 10 μm obtained at ground-level by the combination of particles spectrometers used. The observed size distributions are typically bimodal for the four measurements times shown, with the first modal radius between <0.015 and 0.4 μm, hereafter referred to as fine mode, and the second between 0.5 and >10 μm, referred to as coarse mode. Between these modal values generally there is a minimum (inflection point), corresponding to a radius of about 0.4 μm. As it can be seen in Fig. 3, volume size distribution measured on the 27 October reveals a high value for the coarse mode, related with the stagnation meteorological situation. On the 28 October, the coarse mode shows smaller values, but the fine mode has increased due to a local pollution event, identified by the high increase in the nitrate concentration. During the 2 to 4 November, size distributions attained lower values, due to the different synoptic situation. Both fine and coarse mode are significantly reduced, even during local pollution events.

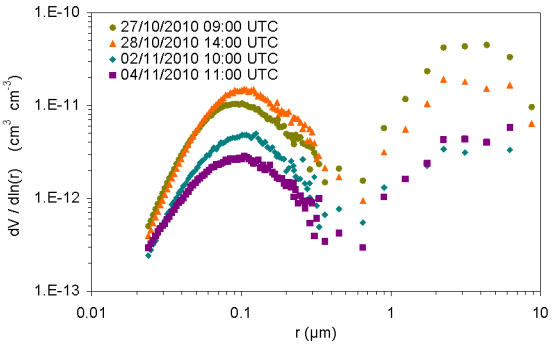

Fig. 3. Log-log plot of the in-situ volume size distribution for 27 October at 9:00 UTC, 28 October at 14:00 UTC, 2 November at 10:00 UTC and 4 November at 11:00 UTC.

3.3 Atmospheric profiles

Atmospheric profile information where obtained from both radiosounding and lidar measurements. Figs. 4 to 6 show profiles corresponding to 27 October, 2 November and 4 November respectively at times when simultaneous measurements were available. On the left hand side of the figures, virtual potential temperature and dew point temperature profiles are plotted up to 8 km height above ground level. The computed height of the planetary boundary layer (PBL) is also marked and can be easily identified as the layer where the virtual potential temperature remains fairly constant with height due to the intensive vertical mixing [40]. The PBL height was also compared with the one based on the backscatter signal obtained from lidar measurements [41], with satisfactory agreement in all studied cases (not shown). The two central plots show wind direction and wind speed profiles as measured by the radiosonde. Finally, the right hand side represents the aerosol backscatter coefficient profile, where the computed H is indicated. The H values refer to height above ground-level and were used to convert the volume size distribution measured in-situ at ground-level to column-integrated values.

Fig. 4 illustrates radiosounding and aerosol backscatter profiles for 27 October around 9:00 UTC. The temperature profile shows a thermal inversion at 320 m agl, determining the height of the mixing layer at this level. This reduced height, together with the synoptic situation at that time and

the low wind speed near the surface, were responsible for the increased concentration of particles near the surface (Figs. 1 and 2). The backscatter coefficient profile followed a nearly exponential decay with height, with a computed H equal to 1.3 km. In fact, it is important to note that this decay with height is largely more pronounced at low altitude due to the synoptic situation during this date. The profile description for 28 October was very similar to the previous day with a slightly lower mixing layer located at 290 m agl and absence of wind below it, but no backscatter profile data were available on that day.

Atmospheric profiles for 2 November around 10:00 UTC are shown in Fig. 5. The temperature inversion was located at a higher altitude and the computed height of the mixing layer results at 1330 m agl. Wind speed was 4 m s^{-1} within the PBL and increases to 20 and 25 m s^{-1} from 1.5 and 4.5 km altitude respectively. The backscatter profile shows an exponential decrease with height and the computed H locates at 1.1 km agl. Atmospheric profiles for 4 November at 11:00 UTC are presented in Fig. 6 and show similar characteristics as for 2 November. The height of the mixing layer locates at 850 m agl and moderate wind speed dominates within the profile, with and average speed around 4 m s^{-1} in the mixing layer. As in the previos case, the backscatter profile is nearly exponential, with H at 910 m agl. The studied backscatter profiles corresponding to November are less pronounced near the surface than that observed for 27 October. The higher mixing layer during this period at the beginning of November promotes conditions more in concordance with standard atmospheric profiles, with exponential decay of particles throughout the troposphere in the absence of external aerosol intrusions.

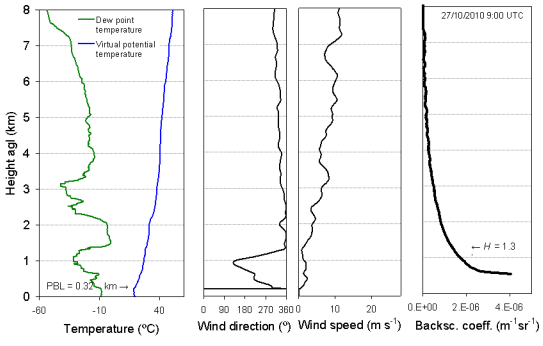

Fig. 4. Atmospheric profile data corresponding to 27 October 2010 at 9:00 UTC from the surface up to 8 km agl. The left-hand side plot shows temperature and virtual temperature profile; the central plots show direction and speed of wind; and the right-hand side plot is the backscatter coefficient profile. Both the mixing height and scale height are also indicated.

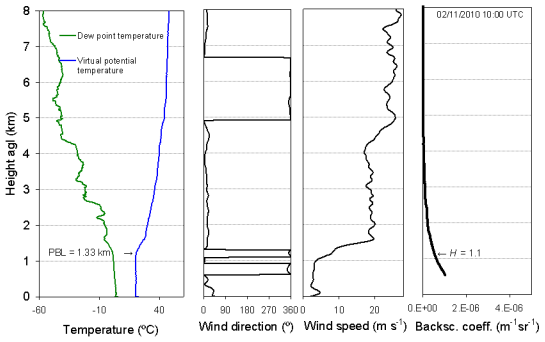

Fig. 5. Same as Fig. 4 but for 2 November at 10:00 UTC.

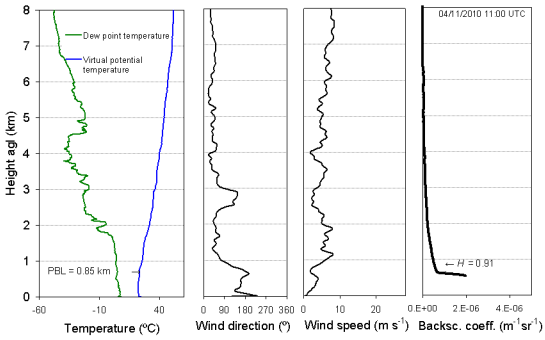

Fig. 6. Same as Fig. 4 but for 4 November at 11:00 UTC.

3.4 Atmospheric Columnar Characteristics

The AODs at 500 mn and Angström exponents (440-1020 nm) for the selected days are shown in Table 1. In spite of the differences in the AOD values, the retrieved Angström exponents are fairly similar with low values above 1.2. Estimates of AOD from aerosol extinction measurements at the surface boundary layer scaled to height by means of H overestimate AOD measured for the atmospheric column during the stagnation period. Data from 2 November at 10:00 UTC, with a well develop mixing layer reaching 1330 m agl, show better agreement compared with the AOD measured for the atmospheric column. For 4 November at 11:00 UTC, when the mixing layer height reaches 850 m agl and in the presence of a cleaner atmospheric profile, the AOD estimate from in-situ data at the surface also overestimates values from the entire column.

Table 1. Atmospheric optical depth at 500 nm and Angström exponent for 440-1020 nm for selected days as computed from sun-photometer measurements.

date	AOD (500 nm)	Angström exponent (440-1020 nm)
27 October at 09:00	0.043	1.203
2 November at 10:00	0.065	1.488
4 November at 11:00	0.022	1.240

Fig. 7 shows aerosol volume size distribution vs. radius between 0.01 and 10 μm, in logarithmic scale, obtained on 27 October at 9:00 UTC. The observed size distributions are typically bimodal, with the first modal radius between <0.015 and 0.4 μm, hereafter referred to as fine mode, and the second between 0.5 and >10 μm, referred to as coarse mode. Between these modal values generally there is a minimum (inflection point), corresponding to a radius of about 0.4 μm. Remote sensing is sensitive to the aerosol optical properties of the entire column, while in-situ instruments measure the aerosols at ground level, which may not be representative of the distributed aerosol in the total boundary layer. As both measuring techniques provide the same shape, it can be concluded that the aerosols contained in the whole mixing layer are similar. On the other hand, the agreement between the volume size distribution provided by the inversion code and that measured at ground-level was poor, raising concern about the validity of the scale height value employed in the conversion of the surface data for intercomparison. The magnitude of the size distribution strongly depends on the scale height chosen.

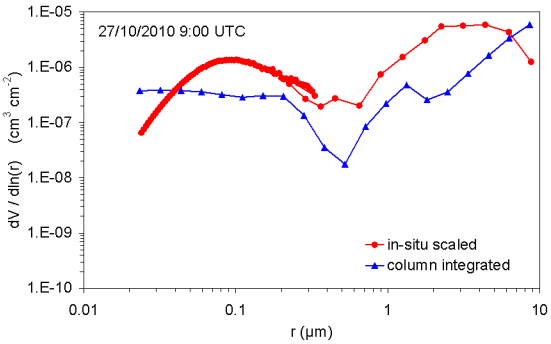

Fig. 7. Log-log plot of the columnar volume size distribution measured at the experimental site on the 27th October at 9:00 UTC. In-situ scaled data refers to in-situ measurements integrated to the column by means of the scale height provided by the lidar, while column integrated refers to data obtained by the inversion method applied to the sun-photometer measurements.

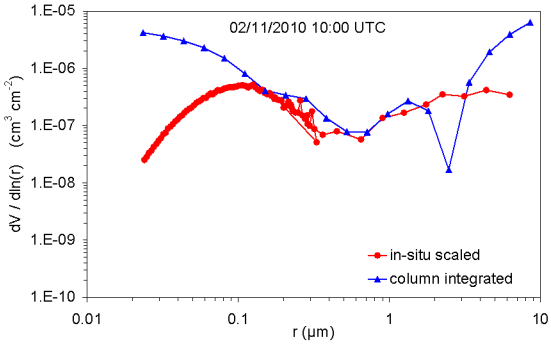

Fig. 8. Same as Fig. 7 but for 2 November at 10:00 UTC.

Fig. 8 shows the size distributions obtained for 2 November at 10:00 UTC, with the same bimodal shape but better agreement in the range from 0.2 to 2 μm. As it was previously mentioned, the inversion will produce a distribution function restricted in particle size because AOD is usually measured in a limited spectral range. This limitation might explain the raising of the column integrated size distribution provided by the cimel instrument. It might be related with assumptions made in the ill-posed inversion of the optical data.

Fig. 9 represents the same information as the former two figures, but for 4 November at 11:00 UTC. In this case, the coarse mode shows better agreement, while the fine mode presents a different shape for the column-integrated size distribution, with a more rounded shape but not in good agreement with the ground-level fine mode.

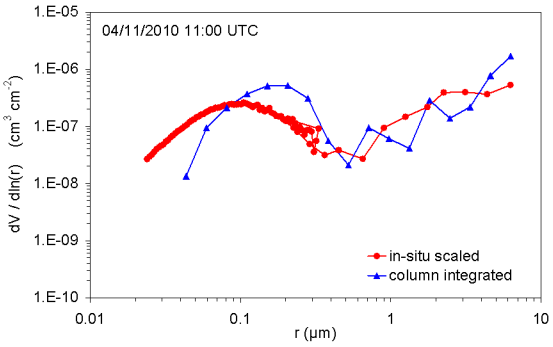

Fig. 9. Same as Fig. 7 but for 4 October at 11:00 UTC.

4 Conclusions

During the SPALI10 field campaign at Madrid, a comparison of columnar versus ground-level measurements of aerosol size distribution was performed. The combination of two particle spectrometers provided size distribution ranging from 15 nm to 10 μm at ground-level. Regarding the column-integrated characterization of the atmospheric aerosol, a sun tracking photometer yields aerosol size distribution using sky radiance measurements in conjunction with solar direct irradiance at several wavelengths. In-situ measurements at ground-level were converted into column-integrated values using the retrieved scale height values provided by lidar profiles under certain assumptions. Two different synoptic situation were analyzed, firstly, a stagnation scenario (27 October), with pollution concentrations growing for one day to the next; secondly, a clean atmosphere scenario (2 and 4 November), dominated by the arrival of Atlantic air masses, with low atmospheric pollution. Aerosol size distribution at ground-level showed bimodal shape in both scenarios, with an inflection point around 0.4 μm. Column-integrated size distributions provided by the sun tracking photometer match this bimodal shape, specially in the size range between 0.2 and 2 μm, where the inversion algorithm is more reliable. On the other

hand, absolute values disagree and the shape of each mode (fine and coarse) did not resemble the ground-level data. A better agreement was found for clean situations when the mixing layer reaches higher altitudes and the aerosol concentration within the atmosphere follows an exponential decay profile with height. In fact, it can be stated that this is very much related with the local aerosol distribution, mainly affected by its origin and the particular atmospheric thermodynamic state.

The atmospheric aerosol concentration in urban areas depends on the intensity of source emissions, chemical processes as well as meteorological conditions. In fact, elevated atmospheric aerosol concentration usually occurs in urban areas during specific meteorological conditions (i.e., near-surface temperature inversion, high pressure system, low wind). The anthropogenic source of aerosol into the atmosphere in absence of a well developed mixing layer is far from homogeneous and not exponentially distributed with height. Moreover, during stagnant periods aerosols are prone to suffer physico-chemical transformations within the PBL, aging and changing their properties. Therefore estimates of columnar aerosol optical and microphysical properties from in-situ measurements at ground-level are not straightforward and the approximation through a scale height fails.

During clean atmospheric situations and with a homogeneous and well developed mixing layer, the observed in-situ aerosol optical and microphysical properties scaled to height provides a good estimate for the entire atmospheric column. Nevertheless, the conversion of in-situ ground-level size distributions to columnar ones may be affected by the uncertainty introduced by the scale height assumptions, explaining the disagreement on absolute values observed.

Further investigations are required to develop appropriate models in order to reduce uncertainties over urban areas and particularly during stagnant periods. New in-situ data and products from sun-photometers networks are becoming widely used; therefore, further studies in a broad range of conditions will contribute to it.

ACKNOWLEDGMENTS

This work was supported by the Spanish Ministry of Science and Technology through projects CGL-2006-27108-E/CLI (DAMOCLES Aerosol Scientific Thematic Network), CGL2008-01330-E/CLI (Spanish Lidar Network), CGL2010-09225, CGL2010-18782 and CSD2007-00067; by the Andalusian Regional Government through projects P10-RNM-6299 and P08-RNM-3568; and by EU through ACTRIS project (EU INFRA-2010-1.1.16-262254). The authors gratefully acknowledge the NOAA Air Resources Laboratory (ARL) for the provision of the HYSPLIT transport and dispersion model.

REFERENCES

[1] B.N. Holben, T.F. Eck, I. Slutsker, D. Tanre, J.P. Buis, A. Setzer, E. Vermote, J.A. Reagan, Y.J. Kaufman, T. Nakajima, F. Lavenu, I. Jankowiak, and A. Smirnov, "AERONET: a federated instrument network and data archive for aerosol characterization", *Remote Sens. Environ.*, vol. 66, pp. 1–16, Oct. 1998.

[2] M. H. Bergin, S.E Schwartz, R.N Halthore, J.A. Ogren, D.L. Hlavka, "Comparison of aerosol optical depth inferred from surface measurements with that determined by sun photometry for cloud-free conditions at a continental U.S. site", *J. Geophys. Res.*, vol. 105, pp. 6807–6816, Mar. 2000.

[3] I. Veselovskii, O. Dubovik, A. Kolgotin, T. Lapyonok, P. Di Girolamo, D. Summa, D.N. Whiteman, M. Mishchenko, D. Tanré, "Application of randomly oriented spheroids for retrieval of dust particle parameters from multiwavelength lidar measurements", *J. Geophys. Res.*, vol. 115, pp. D21203-6, Nov. 2010.

[4] O. Dubovik, A. Smirnov, B.N. Holben, M.D. King, Y.J. Kaufman, T.F. Eck, I. Slutsker, "Accuracy assessments of aerosol optical properties retrieved from Aerosol Robotic Network (AERONET) Sun and sky radiance measurements", *J. Geophys. Res.*, vol. 105, pp. 9791-9806, Apr. 2000.

[5] O. Dubovik, B.N. Holben, T. Lapyonok, A. Sinyuk, M.I. Mishchenko, P. Yang, I. Slutsker, "Non-spherical aerosol retrieval method employing light scattering by spheroids", *Geophys. Res. Lett.*, vol. 29, 10, 10.1029/2001 GL014506, May 2002.

[6] A.I. Bokoye, A. Royer, N.T. O'Neill, P. Cliche, G. Fedosejevs, P.M. Teillet, and L.J.B. McArthur, "Characterization of Atmospheric Aerosols across Canada from a Ground-based Sunphotometer Network: AEROCAN", *Atmos. Ocean,* vol. 39, pp. 429–456, Dec. 2001.

[7] F. Molero, L. Alados-Arboledas, M. Pujadas, A. Alcántara, V.E. Cachorro, V. Estellés, F.J. Olmo, J.A. Martínez-Lozano, J. Lorente, J.P. Díaz, A. Labajo, B. de la Morena, H. Horvath y A.M. Silva. "Comparison of aerosol size distributions measured at ground level and calculated from inversion of solar radiances", Proceedings of SPIE, vol. 5979, *Remote Sensing of Clouds and the Atmosphere X*, K. Schäfer, A.T. Comerón, J.R. Slusser, R.H. Picard, M.R. Carleer, N. Sifakis, eds., pp. 19-22, Sep. 2005.

[8] J. Plaza, M. Pujadas, and B. Artinano, "Formation and transport of the Madrid ozone plume", *J. Air Waste Manage.*, vol. 47, pp. 766-774, 1997.

[9] M. Pujadas, J. Plaza, J. Teres, B. Artinano, and M. Millan, "Passive remote sensing of nitrogen dioxide as a tool for tracking air pollution in urban areas: the Madrid urban plume, a case of study", *Atmos. Environ.*, vol 34, pp. 3041-3056, May 2000.

[10] B. Artíñano, P. Salvador, D.G. Alonso, X. Querol, and A. Alastuey, "Anthropogenic and natural influence on the PM_{10} and $PM_{2.5}$ aerosol in Madrid (Spain). Analysis of high concentration episodes", *Environ. Pollut.*, vol. 125, pp. 453-465, Oct. 2003.

[11] P. Salvador, B. Artinano, D.G. Alonso, X. Querol, and A. Alastuey, "Identification and characterisation of sources of PM_{10} in Madrid (Spain) by statistical methods", *Atmos. Environ.*, vol. 38, pp. 435-447, Jan. 2004.

[12] J. J. Schwab, O. Hogrefe, K.L. Demerjian, V.A. Dutkiewicz, L. Husain, O.V. Rattigan, and H.D. Felton, "Field and laboratory evaluation of the Thermo Electron 5020 Sulfate Particulate Analyzer", *Aerosol Sci. Tech.*, vol. 40, pp. 744-752, Oct. 2006.

[13] R.W. Long, and W.A. McClenny, "Laboratory and field evaluation of instrumentation for the semicontinuous determination of particulate nitrate (and other water-soluble

particulate components)", *J. Air Waste Manage.*, vol. 56, pp. 294-305, Mar. 2006.

[14] S.C. Wang, and R.C. Flagan, "Scanning Electrical Mobility Spectrometer", *Aerosol Sci. Tech.*, vol. 13, pp. 230-240, 1990.

[15] E.O. Knutson, K.T. Whitby, "Aerosol Classification by Electric Mobility: Apparatus Theory and Applications", *J. Aerosol Sci.*, vol. 6, pp. 443-451, Nov.1975.

[16] K. Willeke, P.A. Baron, *Aerosol measurements principles, techniques and applications*, Van Nostrand Reinhold, New York, USA, pp. 143–195, 1993.

[17] H. Grimm, D.J. Eatough, "Aerosol Measurement: The Use of Optical Light Scattering for the Determination of Particulate Size Distribution, and Particulate Mass, Including the Semi-Volatile Fraction", *J. Air Waste Manage.*, vol. 59, pp. 101-107, Jan. 2009.

[18] L. Alados-Arboledas, F.J. Olmo, A. Alcántara, H. Lyamani, J. Lorente, J.A. Martínez-Lozano, V. Cachorro, A. Labajo, B. de la Morena, A. Díaz, M. Pujadas, H. Horvath, A.M. Silva, G. Pavese, "VELETA 2002 field campaign a general overview", *Óptica Pura y Aplicada*, vol.37, pp. 3271–3276, 2004.

[19] L. Alados-Arboledas, H. Lyamani, F.J. Olmo, "Aerosol size properties at Armilla, Granada (Spain)", *Q. J. Roy. Meteor. Soc.*, vol. 129, pp. 1395-1413, Apr. 2003.

[20] C. Gueymard, *SMARTS2, simple model of atmospheric radiative transfer of sunshine: algorithms and performance assessment.* Technical Report FSEC-PF-270-95. Available from Florida Solar Energy Center, Cocoa, FL, USA, 1995.

[21] F.X. Kneizys, E.P. Shettle, L.W.,Abreu, J.H.,Chetwind, G.P. Anderson, W.O. Gallery, J.E.A Selby,.,S.A. Clough, 1988. *Users Guide to LOWTRAN7.* Environment Research Paper 1010, US Air Force Geophysics Laboratory, Bedford, MA, 1988.

[22] T.F. Eck, B.N. Holben, J.S. Reid, O. Dubovik, A. Smirnov, N.T. O'Neill, I. Slutsker, S. Kinne, "Wavelength dependence of the optical depth of biomass burning, urban, and desert dust aerosols", *J. Geophys. Res.*, vol. 104, pp. 31333–31349, Dec. 1999.

[23] V. Estellés, M.P. Utrillas, J.A. Martínez-Lozano, A. Alcántara, F.J. Olmo, L. Alados-Arboledas, J. Lorente, V. Cachorro, H. Horvath, A. Labajo, B.A. de la Morena, J.M. Vilaplana, J.P. Díaz, T. Elias, A.M. Silva, M. Pujadas, "Aerosol related parameters intercomparison of Cimel sunphotometers in the frame of the VELETA 2002 field campaign", *Óptica Pura y Aplicada*, vol. 37, pp. 3289–3295, 2004.

[24] A. Smirnov, B.N. Holben, T.F. Eck, O. Dubovik, I. Slutsker, "Cloud-screening and quality control algorithms for the AERONET database", *Remote Sens. Environ.*, vol. 73, pp. 337–349, Sep. 2000.

[25] T. Nakajima, G. Tonna, R. Rao, P. Boi, Y.J. Kaufman, B.N. Holben, "Use of Sky brightness measurements from ground for remote sensing of particulate polydispersions", *Appl. Optics*, vol. 35, pp. 2672-2686, May 1996.

[26] F. J. Olmo, A. Quirantes, A. Alcántara, H. Lyamani, L. Alados-Arboledas, "Preliminary results of a non-spherical aerosol method for the retrieval of the atmospheric aerosol optical properties", *J. Quant. Spectrosc. Ra.*, vol. 100, pp. 305-314, Jul. 2006.

[27] F.J. Olmo, A. Quirantes, V. Lara, H. Lyamani, L. Alados-Arboledas, "Aerosol optical properties assessed by an inversion method using the solar principal plane for non-spherical particles", *J. Quant. Spectrosc. Ra.*, vol. 109, pp. 1504-1516, May 2008.

[28] F.G. Fernald, B.M. Herman, J.A. Reagan, "Determination of Aerosol Height Distribution by Lidar", *J. Appl. Meteorol.*, vol. 11, pp. 482-489, Apr. 1972.

[29] F.G. Fernald, "Analysis of atmospheric lidar observations: some comments", *Appl. Opt.*, vol. 23, pp. 652-653, Mar. 1984.

[30] J.D. Klett, "Stable Analytical Inversion Solution for Processing Lidar Returns", *Appl. Opt.*, vol. 20, pp. 211-220, Jan. 1981.

[31] J.D. Klett, "Lidar inversion with variable backscatter/extinction ratios", *Appl. Opt.*, vol. 24, pp. 1638-1643, Jun. 1985.

[32] Y. Sasano, H. Nakane, "Significance of the extinction/backscatter ratio and the boundary value term in the solution for the two-component lidar equation", *Appl. Optics*, vol. 23, pp. 11-13, Jan. 1984.

[33] Y. Sasano, E.V. Browell, S. Ismail, "Error caused by using a constant extinction/backscattering Ratio in Lidar solution", *Appl. Optics*, vol. 24, pp. 3929-3932, Nov. 1985.

[34] C. Böckmann, U. Wandinger, A. Ansmann, J. Bösenberg, V. Amiridis, A. Boselli, A. Delaval, F. de Tomasi, M. Frioud, I. Grigorov, A.Hågård, M. Horvat, M. Iarlori, L. Komguem, S. Kreipl, G. Larchevêque, V. Matthias, A. Papayannis, G. Pappalardo, F. Rocadenbosch, J.A. Rodrigues, J. Schneider, V. Shcherbakov, M. Wiegner, "Aerosol lidar intercomparison in the framework of EARLINET: Part II-Aerosol backscatter algorithms", *Appl. Optics*, vol. 43, pp. 977-989, Feb. 2004.

[35] J.L. Guerrero-Rascado, F.J. Olmo, I. Avilés-Rodríguez, F. Navas-Guzmán, D. Pérez-Ramírez, H. Lyamani, L. Alados-Arboledas, "Extreme Saharan dust event over the southern Iberian Peninsula in September 2007: active and passive remote sensing from surface and satellite", *Atmos. Chem. Phys.*, vol. 9, pp. 8453–8469, Nov. 2009.

[36] A. Ansmann, U. Wandinger, M. Riebesell, C. Weitkamp, W. Michaelis, "Independent measurement of extinction and backscatter profiles in cirrus clouds by using a combined Raman elastic-backscatter lidar", *Appl. Opt.*, vol. 31, pp. 7113-7131, Nov. 1992.

[37] R.R. Draxler, G.D. Hess, "An overview of the HYSPLIT 4 modeling system for trajectories, dispersion, and deposition", *Aust. Meteorol. Mag.*, vol. 47, pp. 295–308, Dec. 1998.

[38] R.R. Draxler, G.D. Rolph, *HYSPLIT (HYbrid single-particle Lagrangian integrated trajectory)*, Model access via NOAA ARL READY Website (http://www.arl.noaa.gov/ready/hysplit4.html), NOAA Air Resources Lab., Silver Spring, MD, USA, 2003.

[39] R.R. Draxler, B. Stunder, G. Rolph, A. Taylor, *Hysplit 4 User's Guide*, NOAA Air Resources Laboratory, Silver Spring, MD, USA, 2009.

[40] R.B. Stull, *An Introduction to Boundary Layer Meteorology* pp 233, Kluwer Academic Publishers, The Netherlands, 1988.

[41] H. Baars, A. Ansmann, R. Engelmann, D. Althausen, "Continuous monitoring of the boundary-layer top with lidar", *Atmos. Chem. Phys.*, vol. 8, pp. 7281–7296, Dec. 2008.